Hysteresis cycle in a turbulent, spherically bounded MHD dynamo model

Hysteresis cycle in a turbulent, spherically bounded MHD dynamo model

Klaus Reuter[1,3]**, Frank Jenko**[1] **and Cary B Forest**[2]

[1] Max-Planck-Institut für Plasmaphysik, EURATOM Association,
85748 Garching, Germany
[2] Department of Physics, University of Wisconsin, Madison,
1150 University Avenue, Madison, WI 53706, USA
E-mail: khr@ipp.mpg.de

Abstract. We report direct numerical magnetohydrodynamic simulations at low magnetic Prandtl numbers of a turbulent two-cell flow in a bounded, spherical geometry, driven by a constant body force. The flow amplifies infinitesimal magnetic perturbations if the magnetic Reynolds number Rm is larger than a threshold Rm_c, resulting in a self-excited equatorial magnetic dipole. However, finite amplitude perturbations to the magnetic field can trigger dynamo action below Rm_c: a hysteresis cycle has been found that can sustain dynamo action in an interval $Rm_0 < Rm < Rm_c$. The instability is therefore governed by a subcritical bifurcation. This hysteretic behaviour is associated with changes in the turbulent velocity field caused by the finite amplitude magnetic field. It is then shown that the dynamo state can be accessed by transiently applying a magnetic field from an external source. Finally, a dynamo state with characteristics different from the self-excited case is found in the vicinity of Rm_0.

[3] Author to whom any correspondence should be addressed.

IOP Institute of Physics Φ DEUTSCHE PHYSIKALISCHE GESELLSCHAFT

Contents

1. Introduction

The dynamo process is commonly accepted to be the cause of the magnetic fields observed in planets, stars, galaxies and galaxy clusters [1]–[3]. Dynamo theory explains the amplification of magnetic fields as an instability which occurs in flows of electrically conducting fluids like liquid metals or plasmas [4, 5]. During the last decade, experimental dynamos using liquid sodium were successfully realized in the laboratory [6]–[10]. Both in nature and in recent dynamo experiments, those flows are highly turbulent.

Dynamo action is possible if a nonzero seed magnetic field is present and the induction from flow can overcome ohmic dissipation, i.e. if the magnetic Reynolds number is larger than a certain, critical value Rm_c [4]. Then, the system may undergo a transition to an unstable state with growing magnetic eigenmodes. The dynamo threshold Rm_c has been shown to depend on the strength of turbulence, quantified by the fluid Reynolds number Re (see, for example, [11, 12]). From the point of view of stability theory [13], the transition to self-excitation in the presence of an infinitesimal seed magnetic field is supercritical in dynamo experiments and in most models, resulting in a unique, flow-dependent critical magnetic Reynolds number [14]. However, it is also possible that the dynamo transition can be subcritical; a finite (growing) magnetic field might reduce the hydrodynamic turbulent fluctuations and thus sustains dynamo action for magnetic Reynolds numbers Rm with $Rm_0 < Rm < Rm_c$ [14]. Subcriticality in numerical magnetohydrodynamic (MHD), dynamos was most recently reported for a turbulent flow using a Taylor–Green (TG) forcing [14] (cf also the references therein), and for Keplerian shear flows [15]. However, there are significant differences between the two models which are noteworthy here. In the first case [14], there is a finite Rm_c above which the system becomes linearly unstable with respect to infinitesimal magnetic perturbations; subcriticality

in this context means that a finite amplitude magnetic disturbance causes dynamo action to occur below Rm_c, mediated by nonlinear effects of the Lorentz force on the flow. In the second case [15], the system is linearly stable. The nonnormality of the linear operator in the induction equation may cause transient field growth which eventually must decay in the absence of a nonlinearity. However, if the transiently growing field is strong enough in the presence of the nonlinearity, the latter may become non-negligible and trigger a self-excitation process. There is no kinematic regime, as the system bifurcates under finite amplitude magnetic perturbations 'from infinity,' and is thus subcritical. Subcriticality associated with hysteresis cycles has also been studied in the hydrodynamic context, e.g. in a von Kármán-type experimental swirling flow [16]. Furthermore, subcriticality was studied in numerical models of the geodynamo. Utilizing the fact that these rotating convective dynamos often have axial dipolar solutions, runs were initialized with dipolar magnetic field components to save computing time [17].

In this work, we numerically study the nature of the dynamo bifurcation of a turbulent two-cell flow within a sphere, driven by a constant body force. In section 2, the numerical model is presented. In section 3, the system's hysteretic behaviour is explored by increasing the magnetic diffusivity during the stationary state of a self-excited dynamo (decreasing the magnetic Reynolds number below Rm_c). This follows and extends the recent results found in unbounded TG flow in an infinite, periodic box [14]. Three series of runs at different Reynolds numbers are reported. Then, the flow is studied in the presence of applied magnetic fields of finite amplitude. Section 4 discusses the hysteretic behaviour, identifying a global subcritical bifurcation. The magnetic and velocity fields are analysed by means of visualization and spectral analysis. A comparison is drawn with the TG dynamo, which has been discussed in several publications. The paper closes with a summary in section 5.

2. Model equations

In the case of an incompressible conducting fluid, the magnetic (**B**) and velocity (**v**) fields are governed by the equations of incompressible MHD:

$$\frac{\partial \mathbf{B}}{\partial t} = \nabla \times (\mathbf{v} \times \mathbf{B}) + \lambda \nabla^2 \mathbf{B}, \tag{1}$$

$$\frac{\partial \mathbf{v}}{\partial t} + (\mathbf{v} \cdot \nabla)\,\mathbf{v} = \mathbf{j} \times \mathbf{B} + \nu \nabla^2 \mathbf{v} - \nabla p + \mathbf{F}, \tag{2}$$

$$\nabla \cdot \mathbf{B} = 0, \tag{3}$$

$$\nabla \cdot \mathbf{v} = 0. \tag{4}$$

Here, λ is the magnetic diffusivity, $\mathbf{j} = \mu_0^{-1} \nabla \times \mathbf{B}$ is the current density, ν is the viscosity, p is the pressure and $\mathbf{F}$ is a forcing term. A constant mass density $\rho = 1$ is assumed. In nondimensional units, the problem is characterized by two control parameters, the Reynolds number $Re = LV\nu^{-1}$ and the magnetic Reynolds number $Rm = LV\lambda^{-1}$, which quantify the ratio of advection to viscous dissipation and the ratio of induction to ohmic dissipation, respectively. The variables L and V denote the length and velocity scales, which are characteristic of the system under consideration. The magnetic Prandtl number $Pm = Rm/Re = \nu/\lambda$ quantifies the ratio of viscous to ohmic dissipation.

We use the parallel DYNAMO code to simultaneously solve (1)–(4) in a bounded, spherical geometry [12, 18]. The code employs a standard pseudo-spectral method based on vector

spherical harmonics. The driving is implemented as a constant body force **F**, designed to produce a flow consisting of two counter-rotating cells with a topology similar to that of the flow in the Madison dynamo experiment [12], [19]–[22]. In a centred, cylindrical coordinate system (ρ, ϕ, z), where the z-axis corresponds to the straight line defined by $(\theta = 0)$ in spherical coordinates, the body force reads

$$F_\rho = 0, \quad F_\phi = \epsilon \, \mathrm{sgn}(z) \rho^3 r_\mathrm{d}^{-3} \sin \frac{\pi \rho}{2 r_\mathrm{d}} + \gamma, \quad F_z = (1 - \epsilon) \mathrm{sgn}(z) \sin \frac{\pi \rho}{r_\mathrm{d}} + \delta. \tag{5}$$

Assuming a sphere of radius $r = 1$, the driving is applied within the region $0.25 < |z| < 0.55$, $\rho < r_\mathrm{d} = 0.29$. The parameters were kept constant at $\epsilon = 0.1$, $\gamma = 0.05$ and $\delta = 0.3$. Due to the dominant spectral components of the resulting velocity field, the flow is commonly referred to as a $s2t2$ flow. The origin is resolved, and boundary conditions at the wall are a zero-slip condition for the velocity field, and a potential field for the magnetic field, assuming the outside of the spherical domain to be current free. Similar, analytically constructed, time-independent flows, were studied kinematically in [23].

In the simulation code, the time variable is normalized to a characteristic timescale of the magnetic field, which is the resistive diffusion time, $\tau_\sigma = \mu_0 \sigma r^2$. The relation to one eddy turnover time τ_ν, which is a characteristic hydrodynamic timescale, is given by $\tau_\nu = Rm^{-1} \tau_\sigma$. Hence, in the regime $Rm > 100$, where the runs presented below were performed, the hydrodynamic timescale is faster than the magnetic timescale by two orders of magnitude. We set the characteristic length scale L equal to the radius r of the sphere, which is unity in our simulations. Following an established convention, the characteristic velocity is chosen as the time-averaged rms velocity $V = \sqrt{\overline{\langle |\mathbf{v}|^2 \rangle}}$, where the overbar denotes temporal and the $\langle \cdot \rangle$ operator denotes spatial averaging. The time averaging is performed during the kinematic phase of a run, i.e. when the backreaction of the magnetic field on the flow is negligible.

The numerical resolution used in the simulations is characterized by the number of radial grid points n_r in physical space and the maximum degree n_1 above which the spherical harmonic expansions are truncated. To assure dealiasing, the number of angular points is chosen as $n_\theta = 3/2 n_1$ and $n_\phi = 3 n_1$. Since finite differences are used in radial direction, the value of n_r is required to exceed n_1 by a factor of 4 for reasons of accuracy. In addition, the radial domain decomposition used in our parallel code requires n_r to be divisible without remainder by the number of processors. Two methods are simultaneously used to monitor a run. Firstly, the power balances obtained from the induction and momentum equations (1) and (2) are calculated and required to deviate by less than 1%. Secondly, the kinetic and magnetic spectral energies in terms of the degree l are required to drop at least by a factor of 100 from their maxima (in our model typically found at $l = 2$ and $l = 1$, respectively) to the cut-off n_l. This rule is known from geodynamo simulations which use very similar numerical methods [17]. In the following, the resolutions are given at the beginning of sections 3.1–3.3, where three series of runs at different Reynolds numbers are presented. In addition, a convergence check of the runs at the largest Reynolds number is given in section 3.5. Spectra are presented in section 4.2.

3. Hysteretic behaviour of the turbulent $s2t2$ dynamo

Previously, the stability of an electrically conducting, turbulent $s2t2$ flow under infinitesimal magnetic perturbations was studied numerically [12, 24]. In the computationally accessible regime, the stability curve Rm_c was determined as a function of the Reynolds number Re. It

IOP Institute of Physics Φ DEUTSCHE PHYSIKALISCHE GESELLSCHAFT

Table 1. Series A: simulations performed at $Re = 770$. Unquenched runs are marked with an asterisk. Run A8* provides the initial conditions for the quenched runs A0–A7. The following variables were determined during the statistically stationary state reached after a short transient: $\overline{E_{\mathrm{mag}}}$ and $\overline{E_{\mathrm{kin}}}$ are the time-averaged magnetic and kinetic energies, B is the magnetic field amplitude, δ and δ_2 are measures of the intensity of turbulent fluctuations of B and V, as defined in (7).

Run	Rm	$\overline{E_{\mathrm{mag}}}$	$\overline{E_{\mathrm{kin}}}$	$\overline{E_{\mathrm{mag}}}/\overline{E_{\mathrm{kin}}}$	B	$\delta(B)$	$\delta_2(B)$	$\delta(v)$	$\delta_2(v)$
A0	86	0.00	0.76	0.00	0.00	–	–	1.34	0.25
A1	88	0.09	0.56	0.15	0.42	10.23	0.86	1.30	0.45
A2	89	0.11	0.51	0.22	0.47	5.29	0.71	1.36	0.55
A3	90	0.21	0.31	0.70	0.65	1.25	0.25	1.21	0.61
A4	107	0.23	0.28	0.84	0.68	1.86	0.36	1.33	0.77
A5	128	0.25	0.28	0.87	0.70	2.42	0.42	1.46	0.95
A5*	128	0.00	0.76	0.00	0.00	–	–	1.35	0.24
A6	150	0.29	0.25	1.15	0.76	2.11	0.51	1.37	0.84
A7	171	0.30	0.25	1.22	0.78	2.06	0.40	1.37	0.68
A7*	171	0.00	0.76	0.00	0.00	–	–	1.35	0.24
A8*	214	0.33	0.25	1.30	0.81	1.47	0.40	1.38	0.56

was found that Rm_{c} rises linearly with Re. Furthermore, the results of ongoing work indicate that Rm_{c} flattens at higher Re. A detailed report will be published elsewhere. The stability curve is in qualitative agreement with several numerical studies on mean-field and small-scale dynamos performed in infinite periodic boxes (for more details, see, e.g. [11], [25]–[29]).

In the present paper, we address the nature of the dynamo transition by suddenly increasing the magnetic diffusivity thereby reducing ('quenching') the magnetic Reynolds number below Rm_{c} during the saturated phase of a dynamo that initially has $Rm > Rm_{\mathrm{c}}$. This procedure is repeated for multiple Rm values at three different Reynolds numbers. The corresponding runs are summarized in the following three sections. In addition, we study the behaviour of the system at $Rm < Rm_{\mathrm{c}}$ in the presence of externally applied magnetic fields in section 3.4. A convergence check is presented in section 3.5. A discussion of the observed effects follows in section 4.

3.1. Runs at $Re = 770$ (series A)

A series (referred to as series 'A') of dynamo simulations at different Rm, but with $Re = 770$ held fixed is summarized in table 1. No external field was applied. The grid resolution is $n_{\mathrm{r}} = 480$ and $n_1 = 25$. A convergence check is presented in section 3.5.

Time traces of kinetic and magnetic energies for a subset of the runs are presented in figure 1. Since the magnetic Reynolds number was changed during some of those runs, the time variable is given in λ-independent units of eddy turnover times, $\tau_\nu = Rm^{-1}\tau_\sigma$. Each of the runs was continued for several magnetic diffusion times after the quenching was applied. Run A8*, performed at $Rm = 214$ and shown in panel (a), is a standard dynamo transition in
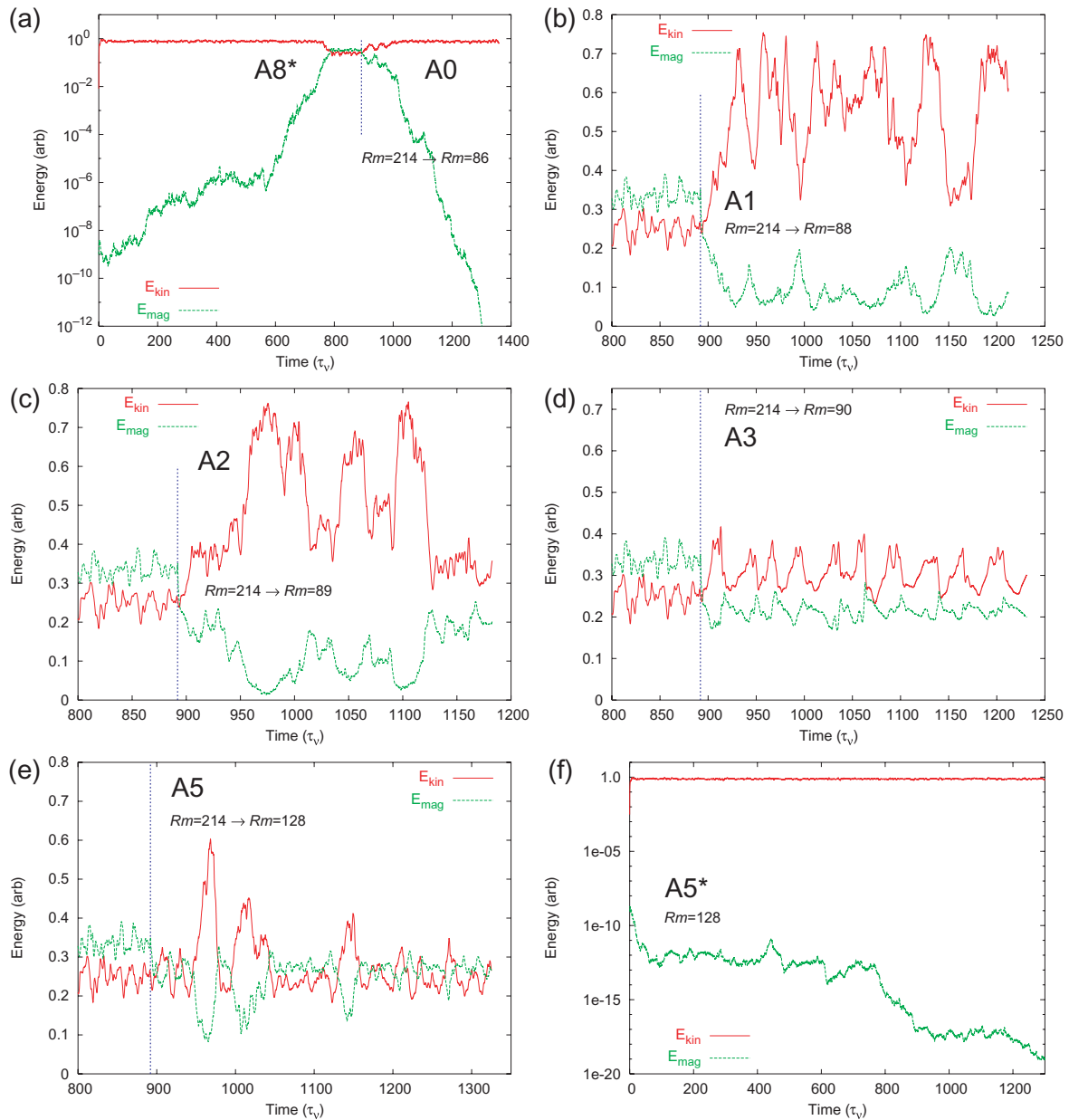
Figure 1. Time traces of kinetic and magnetic energies from a subset of runs at $Re = 770$. (a) A run is started at $t = 0$ with $Rm = 214$ (A8*). During the kinematic phase, the magnetic energy grows exponentially. Starting from $t \approx 775$, the magnetic field is strong enough to react back on the velocity field. In the following, nonlinear saturation occurs. At $t = 892$, the dynamo is quenched to $Rm = 86$, its positive feedback mechanism breaks down, and the magnetic field energy decays exponentially. (b) Starting from the saturated run A8*, the magnetic Reynolds number is reduced to $Rm = 88$ (A1). The dynamo action persists, the system reaches a new quasi-stationary state. (c)–(e) The dynamo is quenched to $Rm = 89$ (90 and 128) and $Rm < Rm_c$. (f) For direct comparison with case (e), the seed magnetic field decays in a run which is performed at $Rm = 128$, starting at $t = 0$.
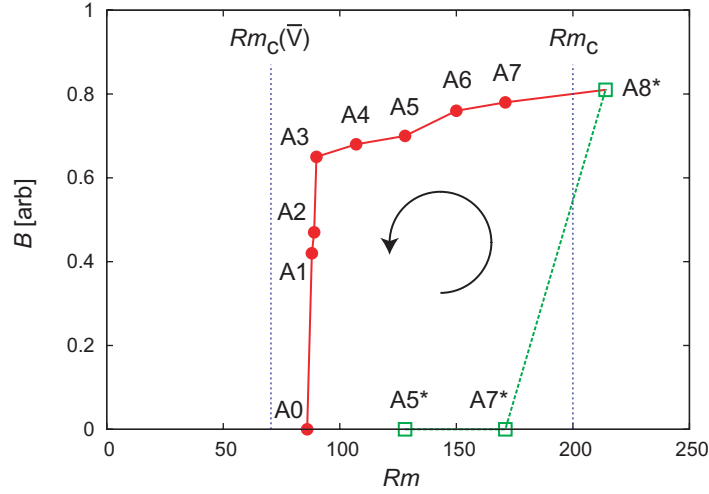
Figure 2. Magnetic field amplitude B as a function of the magnetic Reynolds number Rm for the runs in series A. The red (solid) dots denote the quenched states, starting from the unquenched A8*. For comparison, the green (open) squares show unquenched runs below and above the dynamo threshold at $Rm_c \approx 200$, the latter being indicated by the right vertical blue (dashed) line. A hysteresis cycle in counterclockwise direction results. Furthermore, the critical magnetic Reynolds number $Rm_c(\bar{V}) \approx 70$ of the mean flow from run A5* is shown by the left vertical blue (dashed) line.

which an infinitesimal seed magnetic field grows in time when $Rm > Rm_c$. During the kinematic phase, where the backreaction of the magnetic field is negligible, the magnetic field grows exponentially after an initial transient. Starting from $t \approx 775$, the magnetic field is strong enough to affect the flow via the Lorentz force, leading to nonlinear saturation. The system reaches a quasi-stationary state, which is visible in better detail in the left sections of panels (b)–(e). At $t = 892$, the magnetic diffusivity of the fluid is suddenly increased, corresponding to a decrease of the magnetic Reynolds number down to $Rm = 86$ (run A0), which is below the dynamo threshold $Rm_c \approx 200$. As it is evident from the right section of panel (a), the dynamo can no longer sustain its positive feedback loop. The magnetic energy decays exponentially. Panels (b)–(e) show data from the runs A1–A3 and A5, where dynamo action persists after the system was quenched to $Rm = 88$ (89, 90 and 128), $Rm < Rm_c$. Panel (f) shows timetraces of the kinetic and magnetic energies in run A5*, which was performed at $Rm = 128$. For direct comparison with case A5 no quenching was applied and the seed magnetic field decays.

In figure 2, the magnetic field amplitude $B = \sqrt{2\overline{E_{mag}(t)}}$ during the quasi-stationary state of the runs in series A is plotted as a function of the magnetic Reynolds number. Here, $\overline{E_{mag}(t)}$ is the time-averaged magnetic energy. The critical magnetic Reynolds number Rm_c is also indicated. It was determined via linear interpolation between the growth rate of a dynamo case ($Rm > Rm_c$), and the decay rate of a non-dynamo case ($Rm < Rm_c$). Furthermore, we have computed the mean flow

$$\overline{\mathbf{V}(\mathbf{x})} = \frac{1}{T} \int_{t_0}^{t_0+T} \mathbf{v}(\mathbf{x}, t)\, \mathrm{d}t, \tag{6}$$

Table 2. Series B: runs performed at $Re = 410$. Unquenched runs are marked with an asterisk. Run B10* constitutes the initial condition for the quenched runs.

Run	Rm	$\overline{E_{\mathrm{mag}}}$	$\overline{E_{\mathrm{kin}}}$	$\overline{E_{\mathrm{mag}}/E_{\mathrm{kin}}}$	B
B0	59	0.00	0.71	0.00	0.00
B1	62	0.00	0.71	0.00	0.00
B2	64	0.07	0.57	0.13	0.38
B3	66	0.00	0.69	0.00	0.00
B4	67	0.10	0.47	0.22	0.45
B5	68	0.00	0.67	0.00	0.00
B6	70	0.14	0.38	0.37	0.53
B7	72	0.20	0.30	0.66	0.63
B8	82	0.23	0.21	1.07	0.68
B8*	82	0.00	0.73	0.00	0.00
B9*	90	0.24	0.21	1.14	0.69
B10*	103	0.25	0.21	1.20	0.71

from run A5*. Here, T denotes an averaging time of several hundred eddy turnover times. We have then used the mean flow in kinematic runs, i.e. integration of equation (1) only, to determine its critical magnetic Reynolds number via the previously described interpolation procedure. The resulting $Rm_{\mathrm{c}}(\bar{\mathbf{V}}) \approx 70$ is included in figure 2 as well. Dynamo action is possible in a window $Rm_0 < Rm < Rm_{\mathrm{c}}$, with $Rm_0 \approx 0.44\,Rm_{\mathrm{c}}$. An analysis of the phenomena linked to this hysteresis cycle is given in section 4.

3.2. Runs at Re = 410 (series B)

Since the turbulence strength influences the dynamo threshold Rm_{c} in our system, we have also performed simulations at lower Reynolds numbers compared with series A. Series B, a set of runs at $Re = 410$, is summarized in table 2. The grid resolution is $n_{\mathrm{r}} = 320$ and $n_1 = 25$. Figure 3 shows the corresponding hysteresis cycle. The dynamo threshold in this case is $Rm_{\mathrm{c}} \approx 90$ (run B9* is a marginal self-excited dynamo), the critical magnetic Reynolds number of the mean flow (obtained by time-averaging the velocity field during run B8*) is $Rm_{\mathrm{c}}(\bar{V}) \approx 59$. As is evident from the (red) solid dots in figure 3, quenched dynamos reach statistically stationary states with finite amplitudes in the interval $Rm_0 \approx 64 < Rm < Rm_{\mathrm{c}}$. The width of the hysteresis cycle is $Rm_{\mathrm{c}} - Rm_0 \approx 26$, with $Rm_0 \approx 0.71\,Rm_{\mathrm{c}}$. However, for Rm values near Rm_0, two runs (B2 and B4) show dynamo action, whereas simulations in the vicinity (B1, B3 and B5) have a decaying magnetic field. In all cases, the time integration was performed at least over three magnetic diffusion times. This 'undecided' behaviour between B2 and B6 in a narrow window of $\Delta Rm < 6$ is probably caused by the fact that the temporal evolution of nonlinear systems like the MHD dynamo is sensitive to infinitesimal changes of the initial conditions. As a result, the lower limit of the hysteresis cycle may be defined as an interval rather than a value Rm_0.

3.3. Runs at Re = 178 (series C)

A third series of runs (labelled 'C') was performed at $Re = 178$ and is summarized in table 3. The numerical resolution is $n_{\mathrm{r}} = 280$ and $n_1 = 20$. The dynamo threshold at $Re = 178$ is $Rm_{\mathrm{c}} \approx 45$. The critical magnetic Reynolds number of the mean flow (obtained by time-averaging the

Table 3. Overview of the runs performed at $Re = 178$ ('series C'). The dynamo run C3* constitutes the initial condition for the quenched runs.

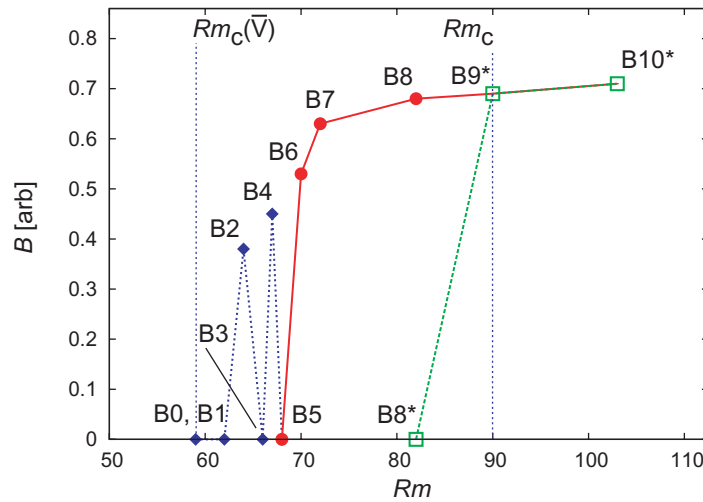| Run	Rm	$\overline{E}_{mag}$	$\overline{E}_{kin}$	$\overline{E}_{mag}/\overline{E}_{kin}$	B
C0	41	0.000	0.51	0.000	0.000
C1	43	0.002	0.52	0.003	0.057
C1*	43	0.000	0.53	0.000	0.000
C2/C2*	45	0.010	0.50	0.020	0.141
C3*	54	0.187	0.26	0.714	0.611

Figure 3. Magnetic field amplitude B of the runs in series B. The red (solid) dots denote the quenched states, starting from B10*. Quenched runs below the decaying run B5 are indicated by blue (solid) diamonds. For comparison, the green (open) squares represent unquenched runs. The vertical blue dashed lines indicate the critical magnetic Reynolds numbers of the time-dependent turbulent flow, and of the mean flow $\bar{V}$ computed from run B8*, respectively.

velocity field of run C1*) is $Rm_c(\bar{V}) \approx 50$. As it is evident from table 3, the hysteresis cycle is comparably narrow in this case. Starting from run C3*, run C1 reaches a stationary state with weak dynamo action at $Rm = 43$. At $Rm = 45$ (C2*), the dynamo does self-excite from an infinitesimal magnetic perturbation, whereas at $Rm = 41$ (C0), the magnetic field decays, starting from finite amplitude. Thus, dynamo action after the quenching is only possible in a narrow window with $Rm_c - Rm_0 < 4$.

3.4. Runs at $Re = 770$ with externally applied magnetic fields

In addition to the previously described *quenched* runs, we have performed simulations at $Re = 770$ and $Rm < Rm_c$ in the presence of an applied $m = 1$ transverse magnetic field. The numerical resolution is $n_r = 480$ and $n_l = 25$. In the simulations presented below, the applied field is perpendicular to the axis of symmetry defined by the forcing, and therefore aligned with the preferred magnetic mode of the system.

Table 4. Overview of the runs performed at $Re = 770$ with an externally applied transverse magnetic field with $B_{apl} = 0.05$ ('series AB'). The second column contains information about the final state of the system after the externally applied magnetic field was switched off, where '–' is a case with a decaying magnetic field.

Run	w/o B_{apl}	Rm	$\overline{E_{mag}}$	$\overline{E_{kin}}$	$\overline{E_{mag}}/\overline{E_{kin}}$	B
AB0	–	43	0.01	0.70	0.01	0.13
AB1	–	47	0.01	0.73	0.02	0.16
AB2	–	68	0.10	0.51	0.20	0.45
AB3	–	77	0.13	0.44	0.30	0.51
AB4	–	81	0.15	0.40	0.39	0.55
AB5	A0	86	0.21	0.31	0.66	0.64
AB6	–	88	0.22	0.26	0.84	0.66
AB7	A2	89	0.23	0.27	0.83	0.67
AB8	A3	90	0.23	0.25	0.94	0.68
AB9	A4	107	0.26	0.22	1.19	0.72
AB10	A5	128	0.28	0.22	1.27	0.75
AB11	A6	150	0.30	0.23	1.28	0.77
AB12	A7	171	0.31	0.24	1.28	0.79

3.4.1. Parameter scan over Rm (series AB). Table 4 gives an overview of the runs performed in series AB, a scan in Rm with a constant applied field. In all cases, the amplitude of the external field was kept constant at $B_{apl} = 0.05$, which corresponds to approximately 6% of the field amplitude during the self-excited run A8*. Once a stationary state was reached, the time integration was continued for one magnetic diffusion time. After that, the applied field was switched off. The dynamo reached the corresponding states from series A as indicated in table 4, except for run AB6, which showed a decaying magnetic field. The magnetic field amplitudes of series AB are plotted in figure 4. For comparison, the respective values from series A and the amplitude of the applied field are included.

3.4.2. Parameter scan over B_{apl}. Finally, we have repeated the run AB9 under variation of the external field's amplitude in order to find the minimum required field strength, which triggers the dynamo transition. We refrain from listing numerical data in a table at this point but rather refer to figure 5. Below the transition, the response amplitudes B of the system are linearly related to the applied field B_{apl}. Point D which is defined by ($B_{apl} = 3.78 \times 10^{-3}$, $B = 0.36$) is marginally below the dynamo transition. Switching off the external field during the stationary phase of run D causes the magnetic field to decay. Starting from point E ($B_{apl} = 5.04 \times 10^{-3}$ and $B = 0.70$), a flat-top indicates nonlinearly saturated dynamo states with the amplitude of simulation AB9. When the applied field is turned off, state A4 is reached from the points E–AB9.

3.5. Convergence test at $Re = 770$ (series AA)

To check the validity of our results, we have repeated some of the runs from series A, keeping $n_r = 480$ fixed but using the higher spectral resolution $n_l = 80$. Table 5 summarizes the results
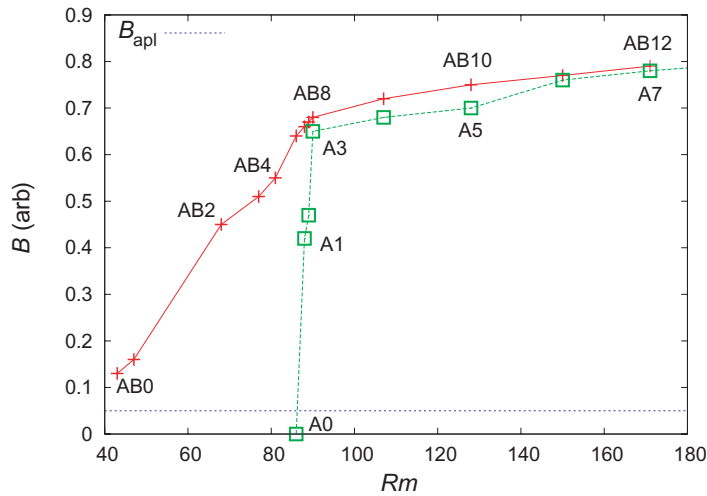
Figure 4. Magnetic field amplitudes during the stationary states of the runs in series AB (red crosses). For comparison, the magnetic field amplitudes from series A are shown (green open squares). The amplitude of the external field applied in series AB is indicated by the blue dotted line.
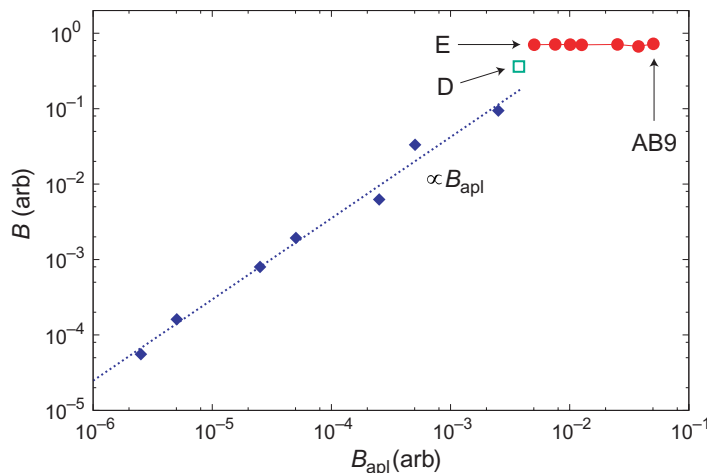

Figure 5. Magnetic field amplitudes in a series of runs at $Rm = 107$ as a function of the applied field's strength. Simulations below the dynamo transition are indicated by blue diamonds. The point D is slightly below the transition. Cases above the transition are shown by red dots. Starting from point E ($B_{apl} = 5.04 \times 10^{-3}$ and $B = 0.70$), dynamos with field amplitudes essentially identical to the one observed in run AB9 are reached.

and allows for direct comparison with table 1. Due to the high computational demands of these runs, the simulations during the statistically stationary states were performed for less than one magnetic diffusion time which was sufficient to calculate averaged energies, but at the same time too short to compute converging δ and δ_2. Run AA3 at $Rm = 90$ is a 'marginal' dynamo and therefore comparable to A1 at $Rm = 88$. It has a smaller magnetic field amplitude and might therefore mark the lower limit of the hysteresis window Rm_0 more accurately than A1. In any case, this would be only a small correction of about 2%. The runs AA5 and AA5*—located

Table 5. Overview of the runs performed at $Re = 770$ ('series AA'). The dynamo run AA8* constitutes the initial condition for the quenched runs AA3 and AA5.

Run	Rm	$\overline{E_{\text{mag}}}$	$\overline{E_{\text{kin}}}$	$\overline{E_{\text{mag}}}/\overline{E_{\text{kin}}}$	B
AA3	90	0.03	0.75	0.04	0.24
AA5	128	0.24	0.29	0.83	0.69
AA5*	128	0.00	0.80	0.00	0.00
AA8*	214	0.31	0.29	1.07	0.79

more central in the hysteresis window—agree well with the corresponding runs A5 and A5*. The self-excited dynamo AA8* shows minor differences in the energy partition compared with run A8*. For a comparison of the corresponding spectra, we refer to section 4.2. To conclude, the runs of series A—and consequently of series B and C—are resolved sufficiently to demonstrate the hysteresis effect.

4. Discussion

In order to better understand the dynamo action at $Rm < Rm_c$, we now interpret and analyse the associated phenomena more closely. Since the runs in series A show the widest hysteresis cycle and are furthermore linked to series AB, we restrict ourselves to a detailed discussion of series A if not stated otherwise. The key questions which arise are the following: why is the system capable of sustaining dynamo action at magnetic Reynolds numbers well below the dynamo threshold Rm_c? What are the differences between these quenched dynamos and cases at comparable Rm which do not self-excite from infinitesimal magnetic perturbations? What characterizes the dynamos in the vicinity of Rm_0 (e.g. A1 and A2) compared with simulations at higher Rm? We define these cases as 'marginal' dynamos due to their location next to Rm_0 and due to their reduced magnetic field amplitudes. Before these questions are addressed, the nature of the dynamo bifurcation which is at the origin of the observed hysteretic behaviour is discussed.

4.1. Subcritical dynamo bifurcation

In the quenched state, the dynamo maintains field amplification against ohmic dissipation in a window $Rm_0 < Rm < Rm_c$, e.g. with $Rm_0 \approx 0.44 Rm_c$ in series A. This happens due to a *finite* amplitude perturbation, which is initially given by the saturated magnetic state of the self-excited, turbulent dynamo at $Rm > Rm_c$ or by the externally applied field. As a result, the system obeys a hysteresis cycle. This behaviour, observed in the runs A1–A7, is evidence of global subcriticality [14] (cf also the references therein). This effect was recently discovered in the turbulent, unbounded TG dynamo [14]. Our studies show that global subcriticality is also present in a less idealized, turbulent dynamo model within a finite, spherical domain. A comparison of both systems will be drawn in section 4.6.

Figure 6 provides an overview of the part of the Re–Rm parameter space, which we have explored in the present study by performing the runs in series A–C. The stability curve Rm_c rises roughly linearly in the covered regime. The lower limit of the subcritical dynamo window Rm_0 rises linearly as well, but with a smaller slope. As a result, the width of the window increases
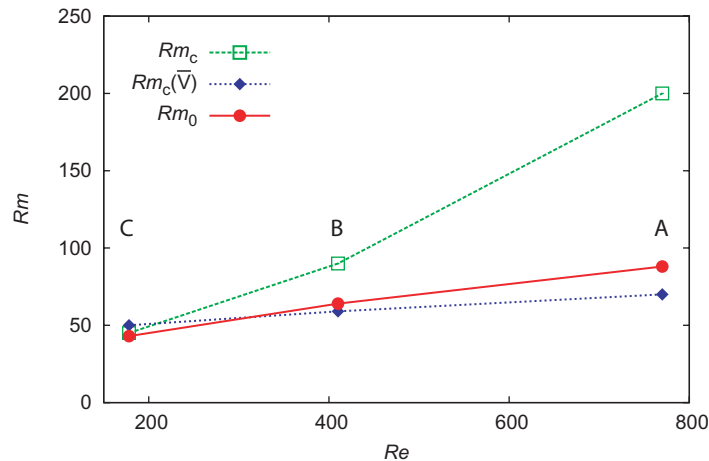
Figure 6. Overview of the dynamo threshold Rm_c and the lower hysteresis limit Rm_0 as functions of Re, based on the data from the series A–C. For comparison, the dynamo threshold of the mean flow $Rm_c(\bar{V})$ (computed from non-dynamo runs) is displayed as well.

with Re. In addition, we have included the dynamo threshold of the mean flow $Rm_c(\bar{V})$. The underlying $\bar{V}$ was computed by time averaging during the non-dynamo runs. The physical mechanisms which govern these stability curves are the focus of ongoing studies. In the present context, the question if the lower threshold Rm_0 saturates with the proposed saturation of Rm_c will be in particular interesting to address.

4.2. Energy spectra of the velocity fields

It is plausible that changes to the flow constitute the memory of the system after the quenching is applied, causing subcritical dynamo action. To check this hypothesis, we have calculated time-averaged energy spectra of the turbulent velocity fields in the simulations A1 (marginal dynamo), A5 (dynamo), A5* (no dynamo) and A8* (self-excited dynamo). The spectra were normalized to unity. Figure 7 shows the result in terms of spherical harmonic degree l and order m. In each case, the spectrum is dominated by the axisymmetric ($m = 0$), two-cell ($l = 2$) component induced by the forcing.

The non-dynamo run A5* has the flattest spectrum, indicative of turbulent fluctuations over a broad range of spatial scales. In the dynamo runs A5 and A8*, the kinetic energy is concentrated at lower mode numbers, consistent with the backreaction of the Lorentz force suppressing small-scale turbulent fluctuations. The upper part ($l > 12$) of the l-spectrum of the marginal state A1 is flatter than the spectra in the dynamo runs, but at the same time steeper than the spectrum in simulation A5*.

In conclusion, the relatively higher amount of energy at small scales in simulation A5* is likely to be the reason why the flow does not self-excite from an infinitesimal seed field. This interpretation is consistent with the idea of an increased magnetic diffusivity due to turbulent mixing ('β-effect'), which effectively increases Rm_c [30].

Figure 8 shows time-averaged spectra of the velocity fields from series AA, which was performed to check the results of series A. At low wavenumbers, no significant differences can
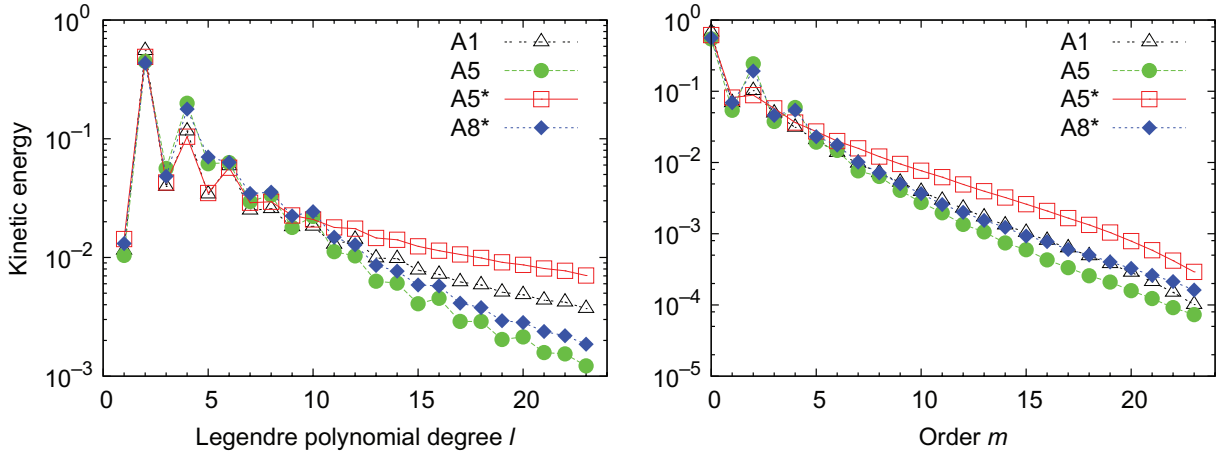
Figure 7. Time-averaged spectra of the velocity fields during the runs A1, A5, A5* and A8*. The spectra are normalized by the total energy.
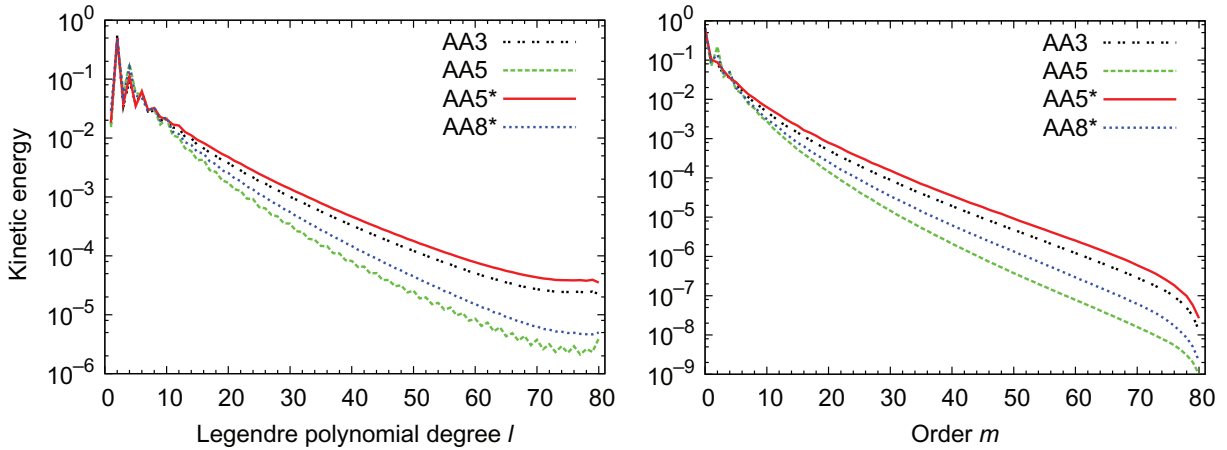

Figure 8. Time-averaged spectra of the velocity fields during the runs AA3, AA5, AA5* and AA8*, which were performed to check the validity of the solutions in series A. The spectra are normalized by the total energy.

be observed. The tails of the spectra in figure 7 are flatter; however, the qualitative behaviour is in good agreement.

4.3. Intensity of turbulent fluctuations

In addition, we have analysed fluctuation properties of the turbulence in the runs of series A. Following [26, 31], two measures are used to globally quantify the level of turbulent fluctuations of a variable $\mathbf{A}$:

$$\delta = \frac{\overline{\langle \mathbf{A}^2 \rangle}}{\langle \bar{\mathbf{A}}^2 \rangle}, \quad \delta_2 = \frac{\sqrt{\overline{\langle \mathbf{A}^2 \rangle^2} - \overline{\langle \mathbf{A}^2 \rangle}^2}}{\overline{\langle \mathbf{A}^2 \rangle}}. \tag{7}$$

Similar to the 'turbulence intensity' measured at a single point in space, the 'noise intensity' δ quantifies the intensity of the turbulent fluctuations globally in the volume under consideration.

Here, the overline denotes averaging in time, the angle brackets averaging in space. The quantity $(\delta - 1)$ is the ratio of the energy in the fluctuations to the energy in the mean field. The variable δ_2 represents the variability of the fluctuations of energy.

In table 1, we have compiled δ and δ_2 associated with the velocity and the magnetic fields. Compared with the values of $\delta(v)$, which are less than 1.5 in all cases, the variable $\delta(B)$ exhibits somewhat larger values during the runs A3–A7, with the largest value $\delta(B) \approx 2.4$ in simulation A5. During the runs A1 and A2, however, the magnetic fields undergo stronger fluctuations, which is indicated by the numerical values of $\delta(B) \approx 10.2$ and $\delta(B) \approx 5.3$, respectively. Given the distinct features of the time-averaged magnetic field in figure 9 below, panels (b) and (d), which were created from the same data set consisting of $\sim$5000 field snapshots sampled over nearly three magnetic diffusion times, these large values cannot be caused by inappropriately short statistics in time. The strong fluctuations are likely to be a general feature of the magnetic field during the marginal dynamo states A1 and A2, linked to a relatively weak backreaction of the magnetic field on the turbulent flow.

4.4. Spatial structure of the magnetic and velocity fields

We have analysed the spatial structure of the time-averaged fields associated with the quasi-stationary states of the runs in series A. The fields corresponding to the marginal dynamos A1 and A2 show peculiar features distinct from the simulations A3–A8*. Below, we focus on a comparison between the marginal dynamo A1 and the self-excited dynamo A8* to work out the characteristics of these states. For that purpose, we have computed time-averaged fields during the quasi-stationary phases. The averaging was performed over several hundred eddy turnover times, which correspond to several magnetic diffusion times, in order to smooth out fluctuations and to assure proper statistics. For visualization purposes, the time-averaged fields were then normalized to unity.

Figure 9 provides a comparison of the magnetic fields. In both cases, the magnetic field is dominated by the ($l = 1$ and $m = 1$) equatorial dipole mode, which is evident from the panels (a) and (b). However, the fields differ in several ways. In the quenched state A1, panel (b), the poloidal field is more concentrated near the equator. Furthermore, the points encircled by magnetic field lines are located closer to the poles, compared with the unquenched state A8*, panel (a). Apart from that, the contours of toroidal flux are differently shaped, and the maxima of toroidal flux are located on contours of opposite sign, when contrasting panel (a) with panel (b). The distinction of the two states is more striking when contours of the modulus of the magnetic field are plotted, as it is done in panels (c) and (d). In the unquenched state A8*, panel (c), the magnetic field amplitude is concentrated on defined areas around the forcing (for details, we refer to figure 10 below, which illustrates the velocity fields), whereas there are comparatively low amplitudes on the equatorial plane. In case A1, panel (d), the magnetic field is more diffused, which results in coherent structures connecting both hemispheres. Separated, coherent structures are located next to the poles. These findings are confirmed by panels (e) and (f) that show volume renderings of the magnetic energy density. We attribute this observation to the relatively larger magnetic diffusivity present in run A1 compared with run A8*.

Figure 10 displays the time-averaged flows during the runs A1 and A8*. Panel (a) shows the velocity field during the saturated phase of the unquenched run A8*, the cross section is aligned with the magnetic dipole. The same is shown in panel (b) for the quenched run A1. Panel (c) shows the same mean flow as panel (a), but with the cross section rotated by $\pi/2$, indicating
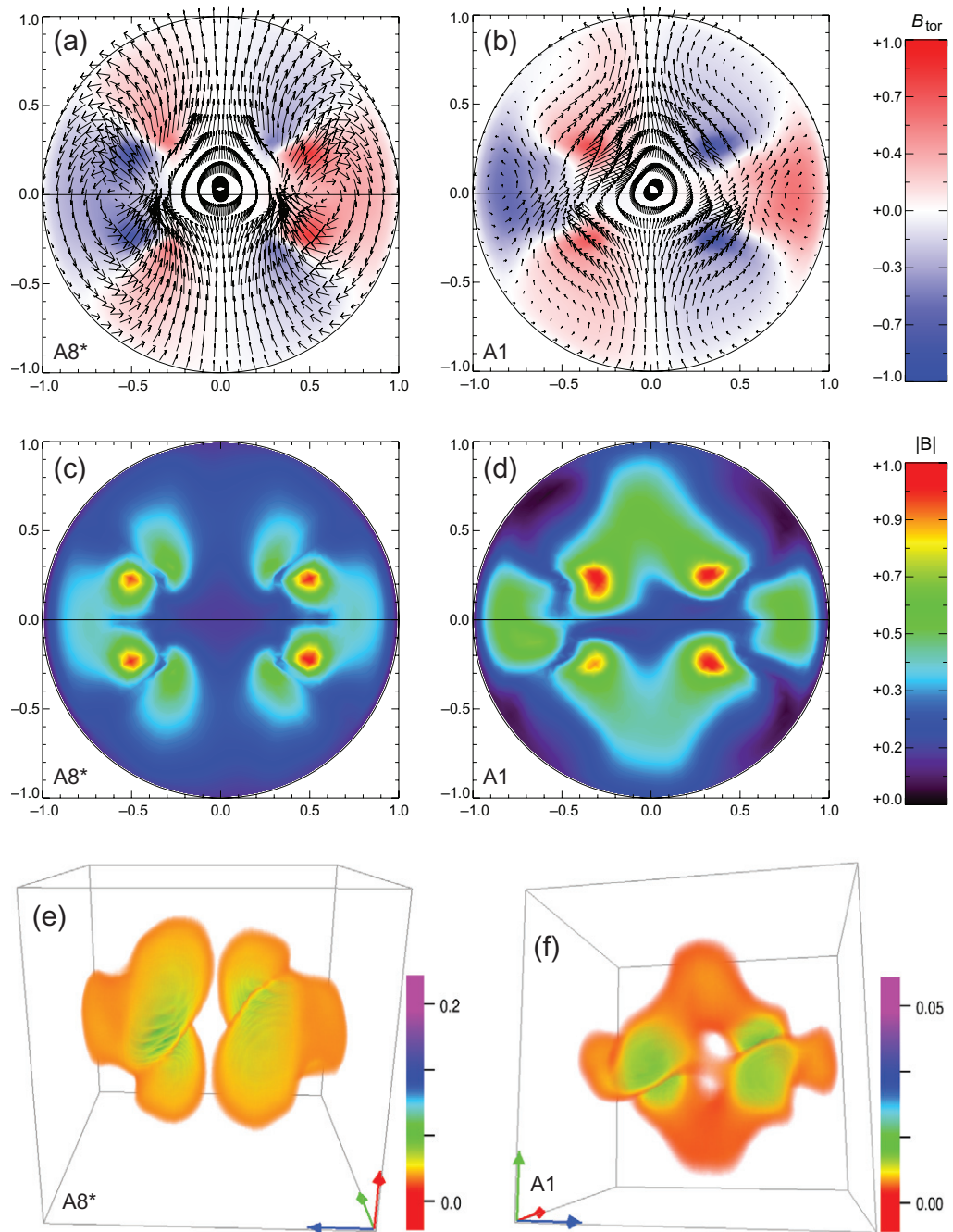
Figure 9. Plots of the magnetic fields that were time averaged during the quasi-stationary phases. The poloidal cross sections are aligned with the dominant ($l = 1$ and $m = 1$) dipolar magnetic eigenmode. (a) Toroidal and poloidal magnetic field components during the unquenched run A8*. (b) Toroidal and poloidal magnetic field components during the quenched run A1. (c) Magnetic field amplitude during run A8*. (d) Magnetic field amplitude during run A1. (e) Magnetic energy density during run A8* (visualization using VAPOR [32]). (f) Magnetic energy density during run A1 (visualization using VAPOR [32]).
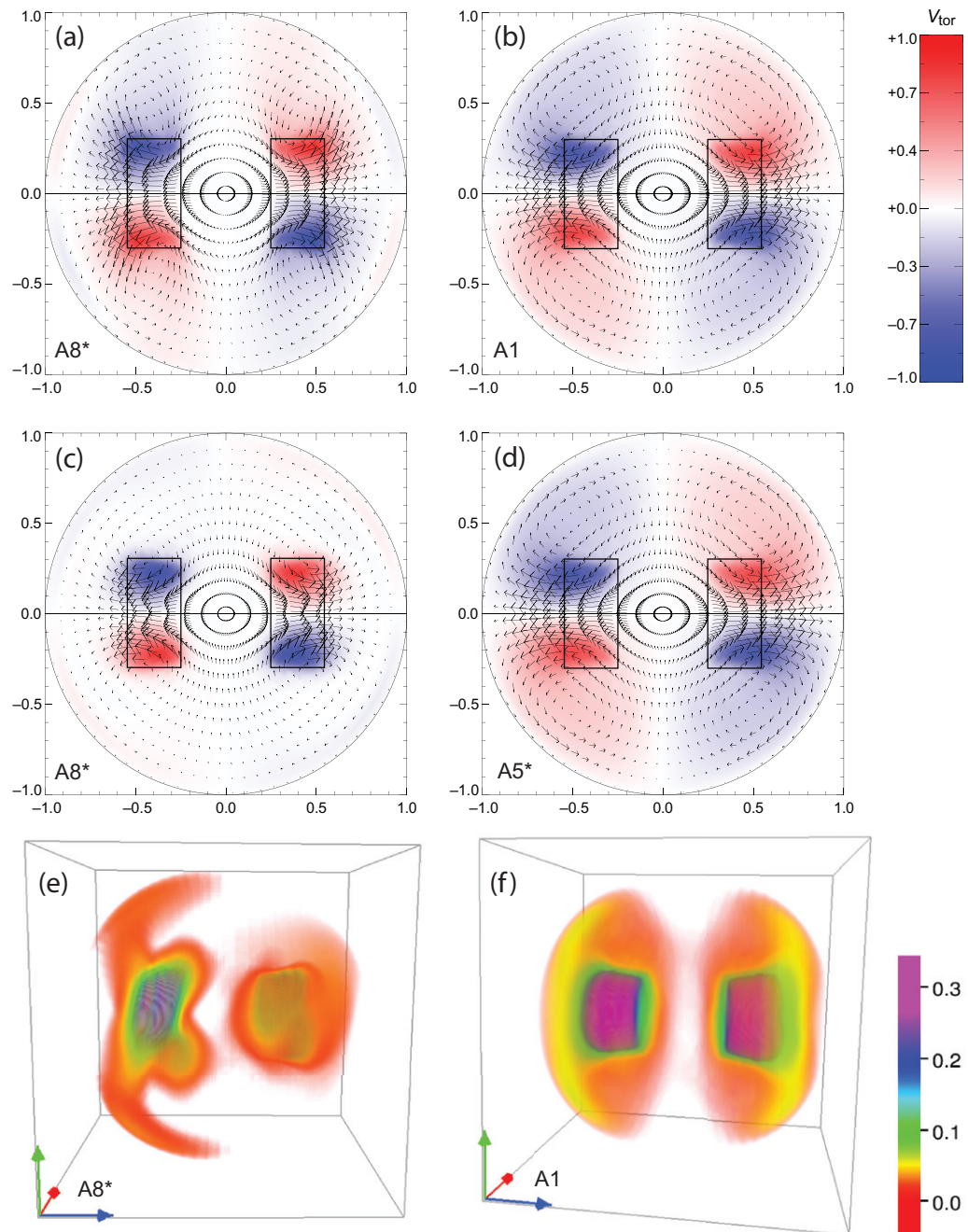
Figure 10. Plots of the velocity fields that were obtained by time averaging during the quasi-stationary phases. For comparison with figure 9, the cross sections (a) and (b) are aligned with the magnetic dipole. In addition, the regions where the forcing (5) is active are indicated by boxes. (a) Toroidal and poloidal velocity field components during the unquenched dynamo run A8*. (b) Toroidal and poloidal velocity field components during the quenched run A1. (c) Like panel (a), however, the cross section is rotated by $\pi/2$. (d) Toroidal and poloidal velocity field components during the unquenched non-dynamo run A5*. (e) Kinetic energy density during run A8* (visulization using VAPOR [32]). (f) Kinetic energy density during run A1 (visulization using VAPOR [32]).

that the rotational symmetry of the mean flow is broken due to the action of the Lorentz force associated with the $m = 1$ dipole. As a result, the mean velocity field in run A8* obeys an $m = 2$ symmetry. Caused by the relatively smaller backreaction of the magnetic field in case A1, its mean flow appears rotationally symmetric. For comparison, the rotationally symmetric mean flow associated with the non-dynamo run A5* is displayed in panel (d). Panels (e) and (f) show the spatial distribution of the kinetic energy density during the runs A8* and A1, confirming the $m = 2$ and rotational symmetries of the flows, respectively.

A direct comparison of the panels (b) and (d) gives evidence that the subcritical dynamo action in run A1, and the suppression of self-excitation from infinitesimal magnetic fields in run A5*, respectively, cannot be explained by modifications to the mean flow. Consequently, the essential changes to the flow in the quenched dynamo state A1 must be small scale and time-dependent and smoothed out by the computation of the mean flows. This is consistent with the findings from section 4.2, where it was shown that the corresponding spectra differ at small scales.

Beyond the insight gained by visual impression, the previously discussed investigations reveal several characteristics of the marginal dynamo in the vicinity of Rm_0 (runs A1 and A2), which are distinct from the dynamo cases at higher Rm (runs A3–A8*). Firstly, the time traces in figure 1, panels (b) and (c), differ from the cases A3 and A5, panels (d) and (e), concerning their amplitudes and fluctuations. This point also becomes apparent in the hysteresis diagram, figure 2. Secondly, the kinetic energy spectrum of run A1 is located in between the dynamo and non-dynamo runs at small scales (large l). Thirdly, the dynamos A1 and A2 are characterized by stronger fluctuations of their magnetic fields, as an analysis of $\delta(B)$ showed.

4.5. Simulations with externally applied magnetic fields

In the previously discussed series A–C, the finite amplitude perturbation that causes subcritical dynamo action is given by the saturated state of a self-excited dynamo. As series AB shows, the latter can be replaced by an externally applied magnetic field, which is parallel to the preferred magnetic mode. As soon as the field is turned off, the dynamo changes its state to the corresponding points of series A. An exception is point A1, which was not reached from point AB6. This indicates that the marginal states in the vicinity of Rm_0 are likely to be metastable.

Starting from point AB12 and going to AB8 in figure 4, the magnetic field amplitudes from series AB follow the hysteresis curve from series A when $Rm > Rm_0$. The behaviour changes below Rm_0, where the amplitudes of the runs AB7 to AB0 do not fall back to the amplitude of the applied field instantly, but rather decrease roughly linearly with a steeper slope. In this regime, the applied field is still amplified, but the flow does not act as a self-sustaining dynamo when the external field is switched off.

We have also studied the role of the orientation of the external field. Instead of $m = 1$ transverse field applied in series AB, we have performed runs at $Re = 770$ with an applied $m = 0$, axial field of equal strength. When the external field is deactivated after a transient, the magnetic fields decay in cases with $Rm < 150$ (cf $Rm < 89$ in series AB). Above this value, states on the hysteresis curve of series A are reached.

Finally, we turn towards a discussion of the minimum field strength required to trigger subcritical dynamo action. For that purpose, a parameter scan over B_{apl} was performed while keeping Re and Rm fixed at the values of run AB9. Below the transition, the field amplitude in the system is a linear function of the applied field strength as indicated by the straight

line in figure 5. Point E marks the critical amplitude $B_{apl,c}$ of the applied field above which nonlinearly saturated dynamo states are reached. The dynamo transition at $Rm_0 < Rm < Rm_c$ in the presence of finite amplitude external fields is therefore governed by a supercritical bifurcation. The numerical value $B_{apl,c} = 5.0 \times 10^{-3}$ is about 0.7% of the total field amplitude reached during the saturated state of run AB9.

It is interesting to relate this dimensionless value to the Madison dynamo experiment. Assuming a sphere of radius $r = 0.5$ m filled with liquid sodium, it translates to a field of $B_{apl,c} \approx 1.72 \times 10^{-3}$ T. In the actual experiment, the Reynolds number is three to four orders of magnitude larger which will—apart from other effects, which are not captured in the simulation—likely to be causing a higher critical amplitude $B_{apl,c}$.

4.6. Comparison with the TG dynamo model

In recent years, the turbulent TG dynamo was the subject of extensive numerical studies [11, 14, 26, 27, 31]. These works were partly motivated by the structural similarity of the TG flow with von Kármán-type experimental swirling flows. The simulations were carried out on three-dimensional (3D) periodic Cartesian grids, which allow the use of efficient pseudo-spectral codes. However, no physical boundaries were considered so far. Therefore, it is interesting to compare the results of these studies with the findings from our model. In addition to the geometric differences, two important differences arise in the boundary conditions: firstly, the no-slip condition on velocity introduces shear layers that are not present in the TG simulations, and secondly, the magnetic field matches to a vacuum solution.

The mean flow $\bar{V}$ changes in our model when Re is increased which is mainly caused by a hydrodynamic instability localized in the boundary layer. As a result, the associated kinematic threshold $Rm_c(\bar{V})$ rises weakly with Re, as shown in figure 6. On the contrary, the values of $Rm_c(\bar{V})$ in the TG case, which limit two separate dynamo windows (a feature which is not present in our model), are only marginally dependent on Re [27]. The lower limit of the hysteresis cycle which is located close to the lower limit of the first kinematic dynamo window shows a similar behaviour.

Compared with DNS data of the unbounded TG flow (as discussed in [26, 31]), the turbulent $s2t2$ velocity field in the sphere is characterized by a comparatively low noise intensity, with $\delta(v, Re = 770) < 1.5$. This is the case throughout the computationally accessible regime and likely to be attributed to the presence of the physical boundary, which constrains the extents of large-scale fluctuations, as visualizations confirm. For the TG case, a monotonically increasing $\delta(v)$ with $\delta(v, Re = 10) \approx 1.5$ and $\delta(v, Re = 100) \approx 3.0$ is reported [26, 31]. Moreover, the saturation of the $\delta(v)$ curve at higher Re was found to be connected to the saturation of the stability curve Rm_c—a scenario which we cannot confirm in our model.

In [14], a dynamo with 'on–off' behaviour is reported in the vicinity of the lower limit Rm_0 of the hysteresis cycle when a magnetic field is applied. However, we do not find this type of dynamo action during the runs performed in series AB. Given the 3D parameter space spanned by Re, Rm and B_{apl}, it is nevertheless possible that 'on–off,' or intermittent dynamo action exists in our model.

Finally, we compare the dynamo states located next to the lower threshold of the hysteresis cycle. In our model, the relatively larger magnetic diffusivity in the marginal dynamo run leads to a less localized magnetic field compared with simulations at higher Rm. However, the magnetic field is a transverse dipole in all cases. In [14], a remarkable change of the magnetic

field's orientation and energy distribution is reported to occur in the vicinity of Rm_0, which the authors link to the dynamo mode in the lower kinematic window of the TG flow.

5. Summary

In this paper, we have numerically shown the existence of a hysteresis cycle of dynamo action in a turbulent, spherically bounded flow at $Pm < 1$. The flow is driven by a constant body force resulting in a mean flow, which consists of two counter-rotating vortices as is the case in the Madison dynamo experiment. The hysteretic behaviour was explored by suddenly decreasing ('quenching') the magnetic Reynolds number Rm below the dynamo threshold Rm_c, starting from the saturated state of a self-excited dynamo ($Rm > Rm_c$), following and extending work based on the TG flow in an infinite, periodic box [14]. This hysteretic behaviour is evidence that the dynamo transition is governed by a subcritical bifurcation.

At $Re = 770$, the quenched system is capable of sustaining dynamo action down to $Rm_0 \approx 88$, which is approximately 44% of the critical magnetic Reynolds number above which self-excitation from infinitesimal seed fields occurs. We find that the flow exhibits two magnetic field configurations in a time-averaged sense, which are both characterized by an equatorial dipole. One mode, which is also the characteristic mode of the self-excited dynamo, appears in a broad range of the quenched regime, down to $Rm \approx 90$. Reducing Rm slightly, one finds the second-dynamo state in a narrow window $88 \lesssim Rm \lesssim 89$. This state is found to be characterized by a smaller field amplitude, by stronger fluctuations, by a changed mean flow, and, on average, by a less localized spatial distribution of the magnetic energy density. The hysteresis behaviour is linked to changes in the turbulent flow, induced by the Lorentz force. Spectra of kinetic energy indicate that the dynamics at intermediate and small scales hinder dynamo action, since these scales are damped during the quenched runs where dynamo action is sustained. The subcritical bifurcation was also studied at lower Reynolds numbers ($Re = 410$ and 178). It was found that the width Rm_c–Rm_0 of the cycle decreases when going to lower Re.

In addition, the system's behaviour was studied in the presence of applied, finite amplitude magnetic fields. It was shown in simulations at $Re = 770$ that an applied equatorial magnetic field is amplified when $Rm < Rm_c$. With $Rm > Rm_0$, the magnetic field amplitude in the system is similar to the field strength observed in the previously discussed hysteresis runs. Reducing Rm below Rm_0 causes the field amplitude to decrease at a steeper slope than the hysteresis curve. Furthermore, when the applied field is turned off in the simulations, the states on the hysteresis curve are reached when $Rm > Rm_0$, otherwise the magnetic field decays. This result is of obvious interest for dynamo experiments where external fields can be applied via coils. It corresponds to an effective reduction of the critical magnetic Reynolds number.

Acknowledgments

IOP Institute of Physics ⦶ DEUTSCHE PHYSIKALISCHE GESELLSCHAFT

References

[1] Roberts P H and Glatzmaier G A 2000 *Rev. Mod. Phys.* **72** 1081
[2] Ossendrijver M 2003 *Astron. Astrophys. Rev* **11** 287
[3] Widrow L M 2002 *Rev. Mod. Phys.* **74** 775
[4] Moffatt H K 1978 *Magnetic Field Generation in Electrically Conducting Fluids* (Cambridge: Cambridge University Press)
[5] Childress S and Gilbert A 1995 *Stretch, Twist, Fold: The Fast Dynamo* (Berlin: Springer)
[6] Gailitis A *et al* 2000 *Phys. Rev. Lett.* **84** 4365
[7] Gailitis A *et al* 2001 *Phys. Rev. Lett.* **86** 3024
[8] Stieglitz R and Müller U 2001 *Phys. Fluids* **13** 561
[9] Monchaux R *et al* 2007 *Phys. Rev. Lett.* **98** 044502
[10] Berhanu M *et al* 2007 *Europhys. Lett.* **77** 59001
[11] Ponty Y *et al* 2005 *Phys. Rev. Lett.* **94** 164502
[12] Bayliss R A *et al* 2007 *Phys. Rev.* E **75** 026303
[13] Manneville P 1990 *Dissipative Structures and Weak Turbulence* (Boston: Academic)
[14] Ponty Y *et al* 2007 *Phys. Rev. Lett.* **99** 224501
[15] Rincon F, Ogilvie G I and Proctor M R E 2007 *Phys. Rev. Lett.* **98** 254502
[16] Ravelet F *et al* 2004 *Phys. Rev. Lett.* **93** 164501
[17] Christensen U, Olson P and Glatzmaier G A 1999 *Geophys. J. Int.* **138** 393
[18] Reuter K *et al* 2008 *Comput. Phys. Commun.* **179** 245–9
[19] Nornberg M D *et al* 2006 *Phys. Rev. Lett.* **97** 044503
[20] Nornberg M D *et al* 2006 *Phys. Plasmas* **13** 055901
[21] Spence E J *et al* 2006 *Phys. Rev. Lett.* **96** 055002
[22] Spence E J *et al* 2007 *Phys. Rev. Lett.* **98** 164503
[23] Dudley M L and James R W 1989 *Proc. R. Soc.* A **425** 407
[24] Reuter K 2006 *Master's Thesis* Universität Ulm
[25] Mininni P D 2006 *Phys. Plasmas* **13** 056502
[26] Laval J-P *et al* 2006 *Phys. Rev. Lett.* **96** 204503
[27] Ponty Y *et al* 2007 *New J. Phys.* **9** 296
[28] Iskakov A B *et al* 2007 *Phys. Rev. Lett.* **98** 208501
[29] Schekochihin A A *et al* 2007 *New J. Phys.* **9** 300
[30] Krause K and Rädler R 1980 *Mean Field Magnetohydrodynamics and Dynamo Theory* (Oxford: Pergamon)
[31] Dubrulle B *et al* 2007 *New J. Phys.* **9** 308
[32] http://www.vapor.ucar.edu